Journal of Advanced Research in Fluid Mechanics and Thermal Sciences

Journal homepage:
https://semarakilmu.com.my/journals/index.php/fluid_mechanics_thermal_sciences/index
ISSN: 2289-7879

Numerical Study on the Impact of the Richardson Number on Convection in an Enclosure, with Moving Sidewalls for Three Aspect Ratios: A = 1, 2 and 0.5

Messai Tarek[1,*], Kholai Omar[2], Boudebous Saadoun[3], Moussaoui Mohammed[4]

[1] Laboratory of Applied Energetics and Pollution, Department of Mechanical Engineering, University of Constantine 1, Constantine, 25000, Algeria
[2] Department of Mechanical Engineering, University of Constantine 1, Constantine, 25000, Algeria
[3] Faculty of Sciences and Applied Sciences, University of Larbi Ben M'hidi, Oum el Bouaghi, 04000, Algeria
[4] Department of Mechanical Engineering, University of Bouira, 10000, Algeria

ARTICLE INFO

Article history:
Received 4 April 2024
Received in revised form 13 August 2024
Accepted 23 August 2024
Available online 15 September 2024

Keywords:
A mixed convection; aspect ratio; critical Richardson number; finite volume method; CFD code; numerical simulation; FORTRAN programming

ABSTRACT

Using mathematical models, this research investigation seeks to explore how varying aspect ratios and the Richardson number impact the mixing effectiveness, fluid flow velocity, and heat transfer characteristics in a rectangle-shaped space where cooling occurs along the sides and warm with a steady temperature exists throughout the 80% of the bottom section's center. Discretizing the governing equations through the finite volume approach, we solved them iteratively using the Tri-diagonal Matrix Algorithm, where pressure-velocity coupling was successfully implemented via the SIMPLER procedure. Innovative approaches for convection and diffusion terms involved employing a power-law difference scheme alongside a central differential scheme. In various simulations with specified parameters (Re = 100, Pr = 0.71), we visualized results in forms like streamlines, isothermal lines, and temperature/velocity profiles, along with local and average Nusselt numbers. We observe five unique structure formations during flow behavior by analyzing how Richardson numbers impact heat transmission within a specific geometric configuration (enclosure size A = 1). A change in aspect ratio leads to improved control over fluid movement while minimizing structural distortion. A subtle rise in heat transmission emerged as the average Nusselt number and Richardson number intersection strengthened force convection's domination while experiencing significant escalation under conditions conductive to natural convection. Decreasing the aspect ratio increased heat transfer efficiency when the Richardson number rose.

1. Introduction

Extending beyond the boundaries of utility, this innovative field touches numerous essential areas with diverse applications, ranging from thermal management to materials science, plus the ever-evolving frontiers of environmental engineering and alternative energy sources and more. Mixed convection's intricate movement within cavities piques researchers curiosity. The value of Ri

* *Corresponding author.*
E-mail address: t.messai@univ-bouira.dz

https://doi.org/10.37934/arfmts.121.1.120136

determines whether mixed convection occurs within the specified range. By mathematical calculation, we determine the degree of involvement between Forceful Convection and Natural Convection. This insight enables us to comprehensively grasp Fluid Dynamics. Since this topic holds great significance on multiple fronts, various investigations have focused on exploring it extensively. A study conducted by Aydin and Yang [1] examined the phenomenon of mixed convection across various cavities, with a heat source positioned near the bottom wall's center. As the heat source traverses the interval spanning 1/5 to 4/5, the movable sides stay cold. Solving this problem, they identified a range of transport regimes according to Richardson number between 0.1 to 10. Throughout this interval of ε = 1/5, similar magnitudes of shearing and buoyancy forces play an amplified role in governing mixed convection. By replicating the conditions set forth in a study by Guo and Sharif [2], they uncovered insights regarding mixed convection behavior within a bounded area. After factoring in various lengths of the heating element, they considered the aspect ratio of the cavity alongside symmetric or irregular placement options. Spanning a dynamic spectrum of Richardson numbers (0.1 to 10), calculations are accurately rendered. Following a thorough investigation, they determined that the outcome comprises two competing vortices whose combined effect ensures uniform temperature distribution over various values of Ri. Using numbers, Aydm [3] investigated how various forces operate within a chamber propelled by sheer force and buoyancy. Under boundary conditions, the moving hot wall rises or falls while the fixed cold wall remains still, with the two parallel walls being adiabatic. He carried out parametric studies with the Gr/Re^2 ratio ranging from 0.01 to 100 for liquids with a Prandtl number equal to 0 and identified three types of heat transfer: Controlled by forced convection, these modes operate in both mixed and buoyancy settings. By contrast, research indicated that the range of mixed convection for Gr/Re2 widens beyond that of the auxiliary float condition. Using advanced mathematical models, scientists Mohamad and Viskanta [4] studied the intricate dynamics caused by the linear motion of fluids within a confined space, where heat is applied from beneath and removed through the movement of an overhead plate. It was established through analysis that the instability manifests itself exclusively in cases where Pr is lower than 0.1 owing to the dominant impact of buoyancy forces in situations involving constant thermal inputs along boundaries.

Researchers Oztop and Dagtekin [5] explored mathematical models of mixed flow within closed chambers containing two walls and a cover. Researching this phenomenon within a symmetrical yet asymmetrical chamber design, they focused on how heat influences fluid flow. Thermal insulation was applied to both the top and bottom surfaces, whereas the lateral moveable partitions had fixed temperature settings. Three distinct wall directions—the impact of which was assessed by checking against Ripple's standards ($0.01 < Ri < 100$), with $Pr = 0.7$ being the crucial factor here - underwent careful scrutiny. Findings demonstrate how the Richardson number and mobile walls' orientation impact fluid movement and temperature passage within enclosed spaces. In whatever direction they advance, the effects of active limits on temperature transport remain alike. Through their numerical analysis, Alleborn *et al.,* [6] investigated various steady two-dimensional flow patterns along with heat and mass transfer under different lid motions. Within a vertically confined space, they identified two pivotal points and fluid behaviors characterized by minimal thermal and mass transport, whereas, near a flat area heated from beneath, they found evidence of oscillations signaled through a Hopf bifurcation, according to Prasad and Koseff [7]. Their experiments investigated combined convective heat transfer phenomena within a container stirred by a lid. Investigators observed a negligible relationship between the Richardson parameter and the heat transfer mechanism after examining Reynolds and physical factors. Numerical simulations carried out by Reima *et al.,* [8] focused on driven-cavity flow in 2D and 3D scenarios under steady temperature gradients. By combining small Richardson values, a mix of convective patterns forms. To probe the effects of

Prandtl number on the cavity's fluid behavior and thermal transfer, Sharif [9] conducted research on laminar mixed convective heat transfer through his experimental setup featuring a moving cover and tiny, horizontal heated boxes that surpassed the temperature of the bottom section. Flow features differ significantly within three unique regimens, including rhythmic behavior near the cool wall due to the separation bubble's influence. Bakar *et al.,* [10] studied numerically analyzes of fluid flow and heat transfer patterns in a two-dimensional cavity with sinusoidal heating. Ferroudj *et al.,* [11] computational study explored fluid movement, heat transfer, and entropy creation due to combined convection. Mixed convection within a square domain was investigated by Ferroudj and Köten [12], Salim *et al.,* [13] made a study on transient laminar mixed convection heat transfer characteristics in a square and cubic shape lid-driven cavity was conducted. The study found that the transition from forced convection to mixed convection occurs at critical Ri numbers of 2.51 and 4.7 for the 3D and 2d cases, respectively. The heat transfer process is strongly affected by the dominant heat convection regime, with the rate of heat transfer increasing in the case of an asymmetric branch dominated by natural convection mode specifically. Based on the previous studies research on mixed convection, we focused through this phenomenon on studying the effect of the Richardson number for three different aspect ratios defined as follows: Isothermal side walls that move independently allow for a comparison between this research and past studies like those conducted by Aydin and Yang [1], as well as mirroring Ferroudj *et al.,* [11] experimental design.

2. Mathematical Formulation

Figure 1 depicts the model utilized in this study. In order to create this model a rectangular cavity was employed, with a fixed length (L) and varying height (H) represented by the aspect ratio A=H/L. The sidewalls of the cavity are maintained at a low temperature (TC) while simultaneously ascending at a velocity (V_0). Positioned in the center of the wall is a heat source spanning 4/5th of its length (ℓ). It remains at a constant temperature (TH). The remaining sections of both the upper walls are thermally insulated. Within this cavity we assume a fluid is incompressible. Additionally, we consider the Boussinesq approximation, which incorporates opposing buoyancy and composition forces within the momentum equations.

$$\rho = \rho_0(1 - \beta(T - T_C)) \tag{1}$$

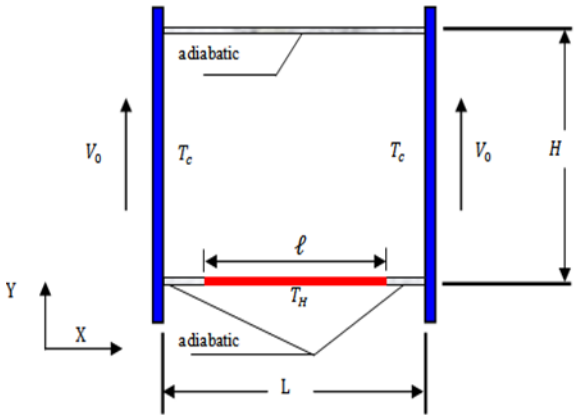

Fig. 1. Schematic diagram of the physical system

The conservation of mass equation, the momentum equations, and the energy equation are the equations that control flow and heat transfer. These are as follows [14]

$$\frac{du}{dx}+\frac{dv}{dy}=0 \tag{2}$$

$$\frac{du}{dt}+u\frac{du}{dx}+v\frac{du}{dy}=-\frac{1}{\rho_0}\frac{\partial p}{\partial x}+\nu\left(\frac{\partial^2 u}{\partial x^2}+\frac{\partial^2 u}{\partial y^2}\right) \tag{3}$$

$$\frac{dv}{dt}+u\frac{dv}{dx}+v\frac{dv}{dy}=-\frac{1}{\rho_0}\frac{\partial p}{\partial y}+\nu\left(\frac{\partial^2 v}{\partial x^2}+\frac{\partial^2 v}{\partial y^2}\right)+g\beta(T-T_c) \tag{4}$$

$$\frac{dT}{dt}+u\frac{dT}{dx}+v\frac{dT}{dy}=\alpha\left(\frac{\partial^2 T}{\partial x^2}+\frac{\partial^2 T}{\partial y^2}\right) \tag{5}$$

Considering the following dimensionless variables:

$$\tau=\frac{V_0 t}{H}, X=\frac{x}{H}, Y=\frac{y}{H}, U=\frac{u}{V_0}, V=\frac{v}{V_0}, P=\frac{p}{\rho_0 V_0^2}, \theta=\frac{T-T_c}{T_H-T_c}, \tag{6}$$

In the presence of the assumptions mentioned above of the adimensional variables, Eq. (1) to Eq. (4) which govern the flow and the thermal transfer are written as follows

$$\frac{dU}{dX}+\frac{dV}{dY}=0 \tag{7}$$

$$\frac{dU}{d\tau}+U\frac{dU}{dX}+V\frac{dU}{dY}=-\frac{\partial P}{\partial X}+\frac{1}{Re}\left(\frac{\partial^2 U}{\partial X^2}+\frac{\partial^2 U}{\partial Y^2}\right) \tag{8}$$

$$\frac{dV}{d\tau}+U\frac{dV}{dX}+V\frac{dV}{dY}=-\frac{\partial P}{\partial Y}+\frac{1}{Re}\left(\frac{\partial^2 V}{\partial X^2}+\frac{\partial^2 V}{\partial Y^2}\right)+Ri.\theta \tag{9}$$

$$\frac{d\theta}{d\tau}+U\frac{d\theta}{dX}+V\frac{d\theta}{dY}=\frac{1}{PrRe}\left(\frac{\partial^2 \theta}{\partial X^2}+\frac{\partial^2 \theta}{\partial Y^2}\right) \tag{10}$$

Eq. (7) to Eq. (10) introduce to us parameters numbers like Prandtl (Pr = ν/α), Reynolds number (Re = V_0L/ν), and Richardson number (Ri = Gr / Re^2). As we delve into these formulas, recognize that Gr's (Gr = $g\beta\Delta TL^3/\nu^2$) importance comes to light. The given parameters serve as the entry point into solving this challenge. The initial and boundary conditions for the current problem are provided in dimensionless form as follows:

Initial condition:

$$\tau=0\ , 0\le X\le 1\ , 0\le Y\le A\quad U=0, V=0, \theta=0 \tag{11}$$

Right and left walls:

$$\tau>0\ , X=0\ \text{ and }\ X=1, 0\le Y\le A\quad U=0, V=1, \theta=0 \tag{12}$$

Top wall

$$\tau > 0 \ ,0 \le X \le 1, Y = A \ \ U = 0, V = 0, \frac{\partial \theta}{\partial Y} = 0 \tag{13}$$

Bottom wall

$$\tau > 0 \ , \frac{(1-\varepsilon)}{2} \le X \le \frac{(1+\varepsilon)}{2}, Y = 0 \ \ U = 0, V = 0, \theta = 1 \tag{14}$$

$$\tau > 0 \ ,0 \le X \le (1-\varepsilon)/2 \text{ and } (1+\varepsilon)/2 \le X \le 1 \ \ Y = 0 \ \ U = 0, V = 0, \frac{\partial \theta}{\partial x} = 0 \tag{15}$$

where ε= ℓ /L=4/5.

The Nusselt numbers, both local and average, for the heated section of the lower wall are expressed as follows

$$Nu(X) = \frac{h\ell}{\lambda} = -\frac{\partial \theta}{\partial Y}\Big|_{Y=0} \tag{16}$$

$$Num = \frac{\bar{h}\ell}{\lambda} = (1/\varepsilon) \int_{(1-\varepsilon)/2}^{(1+\varepsilon)/2} Nu(X) dX \tag{17}$$

For both local and averaged heat transfers, h and $\bar{h}$ represent the relevant coefficients.

In pursuit of computing the averaged Nusselt number, the Simpson's rule serves as a helpful tool during numerical integration processes.

3. Solution Method

By employing the finite volume strategy on the laws of motion (7)–(10), along with the initial and limit conditions have been discretized into a staggered grid. Located throughout the volume are marks indicating U and V, while central storage holds data about P and θ. By leveraging the strengths of PLDS and CDS, we effectively manage multiple processes across diverse domains. Using a time step of $\Delta\tau=10^{-3}$ for each iteration, we employed an implicitly unconditional stability method. Also, the pressure from the continuity equation was calculated using the SIMPLER technique Patankar [15] presented, the algebraic equations that follow take the form:

$$a_P \Phi_P = a_N \Phi_N + a_S \Phi_S + a_E \Phi_E + a_W \Phi_W + \mathrm{S}_\Phi \tag{18}$$

The line-by-line matrix technique (TDMA) was used to solve these equations iteratively along each of the axes, and the relative convergence criterion defined as follows:

$$\xi_\Phi = \left| \frac{(\Phi^{k+1} - \Phi^k)}{\Phi^k} \right| \le 10^{-6} \tag{19}$$

The termination criterion for concluding all computations was established, involving variable Φ (representing U, V,θ) and k is the iteration time number. We developed an in-house FORTRAN program to execute our simulation tasks.

3.1 Grid Independence Test

In this research, the grid mesh utilized in this study was uniform. By assessing the impact of distinct grid configurations on solution quality for Ri = 1 via numerical computations carried out over variously sized grids (from moderate to large), our research revealed insights into the dependability of these methods. Table 1 presents the compiled figures demonstrating unified average Nusselt number. Grid size varies based on A, test data indicates—to hit desired accuracy marks, you need a 130x130 grid (A=1), about 70x140 squares (A=2); going lower still leads to more precise approximations (A=0.5): tolerancing's near 0.06%, 0.05%, or less. We adopted specific grid sizes during this numerical test - Square Cavity A = 1 (130x130), Shallow Cavity A = 2 (70x140), and Tall Cavity A = 0.5 (140x70).

Table 1
Grid independency check for the average Nusselt number at Ri=1, Re=100 and Pr=0.7

A=2	Grid	20×40	40×80	50×100	65×130	70×140
	Num	4.221	4.018	3.983	3.945	3.942
	ARE %	1.84	1.53	0.88	0.45	0.06
A=1	Grid	40×40	80×80	100×100	130×130	140×140
	Num	4.834	4.758	4.739	4.726	4.723
	ARE %	3.45	0.47	0.40	0.07	0.06
A=0.5	Grid	40×20	80×40	100×50	130×65	140×70
	Num	4.497	4.445	4.433	4.422	4.420
	ARE %	1.90	0.40	0.26	0.07	0.05

3.2 Validation

By contrasting our novel approach's outputs against widely recognized standards, we validated the computational model.

3.2.1 First validation

A direct contrast with Aydin and Yang's [1] findings serve as initial validation. The graphical representation provided in Figure 2 highlights the close resemblance between the horizontal velocity projections calculated by Aydin and Yang and those discovered through our investigation.

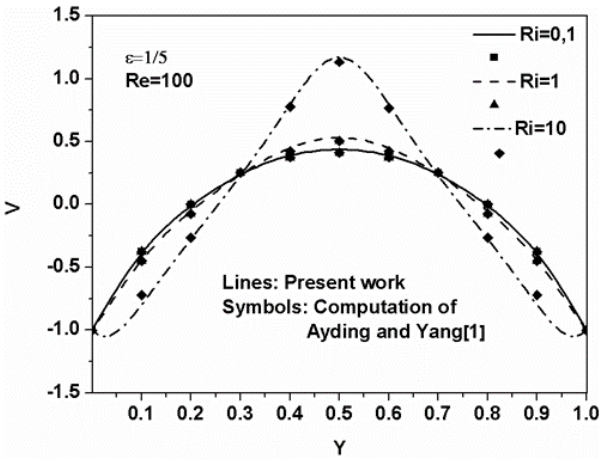

Fig. 2. Comparison between present the code and Aydin and Yang [1]

3.2.2 Second validation

In contrast, we compare our findings to those of Calcagani *et al.,* [16], whose experiments involved a square enclosure with a bottom wall heater that was cooled by adjacent sides. Figure 3 illustrates a close match between the local Nusselt number profile and Gr=1.697×10^5.

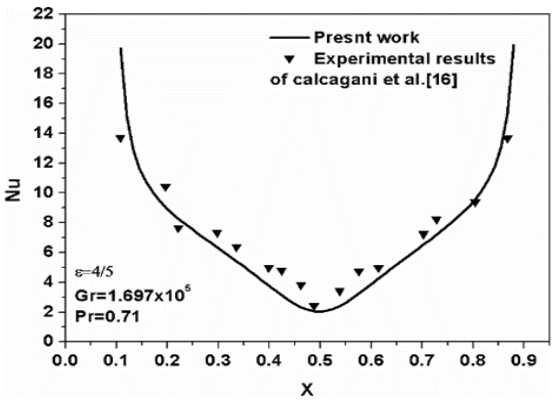

Fig. 3. Comparison of local Nusselt number between our result and Calcagani *et al.,* [16]

4. Results and Discussions

From our investigation comes numerous insights accompanied by appropriate analyses. Investigating the intricate interplay between different elements (A) affecting internal flows and thermal conduction has been our focus. Each aspect ratio was carefully examined: 0.5, 1, and 2. Defined as the proportion between height and width, A takes on great significance. The value assigned to the duration of the warmer area near the base wall is fixed at 0.8 throughout each analysis. Here, we explore how various Richardson numbers (Ri, between 0.05 and 50) affect performance under controlled Reynolds values (Re=100). Our experiment required us to optimize specific parameters such as the time step (10^{-3}) and spatial mesh size configurations for distinct types of cavities. Our investigation into the effects of the Richardson number and aspect ratio on internal cavity flow and heat transfer revealed significant insights. Maintaing a consistent Reynolds number (Re = 100) enables shifts in the Richardson number (Ri) to automatically affect the Grashof number (Gi).

Using multiple graphical representations like streamlines, isothermals, and statistical plots displaying regional and overall Nusselt values, temperature distributions, and velocity maps in the cavity's middle plane, the experiment's discoveries were relayed.

Examining how Richardson numbers affect cavity flow and heating requires thorough research with particular focus. A steady Reynolds number (Re = 100) allows us to investigate the correlation between Grashof number alterations and Richardson number shifts.

By employing these visual representations, researchers gained deeper understanding of the cavity's flow patterns and thermal behavior. Additionally, the average and local Nusselt numbers were examined to assess the heat transfer characteristics. Temperature and velocity profiles in the mid-plane of the cavity were analyzed to further understand the flow behavior. By examining these factors, such as the Richardson number and aspect ratio, the study aimed to provide a comprehensive understanding of their influence on the flow and heat transfer phenomena occurring in the cavity.

4.1 Effect of Richardson Number

In Figure 4 through Figure 6, various parameters are illustrated, including streamlines (Figure 4) and isothermals (Figure 5). Additionally, variations in temperature and vertical velocity within the vertical central plane are depicted (Figure 6(a) and Figure 6(b)). In light of the Richardson number's influence on these realms, five diverse patterns emerge. In cases where Ri≤4.15, let's focus on R = 1. Asymmetric boundary conditions result in division into two oppositely rotating regions - (Ψ_{max} = $|\Psi_{min}|$ = 0.09). Forced convection takes precedence, trailed closely by shearing and buoyant influences; sidewall movement regulates these effects. Boundary layers form nearby due to movement, becoming visible to our observation. In the center of the cavity, the isothermal lines displayed uniform wave shapes due to the screw forces generated by the moving wall panels, causing cold particles to be displaced vertically. Whenever there exist such conditions where the buoyancy forces near the cavity's axis are relatively weaker than those related to shear stress, then heat diffusion satisfaction follows upon wall descent.

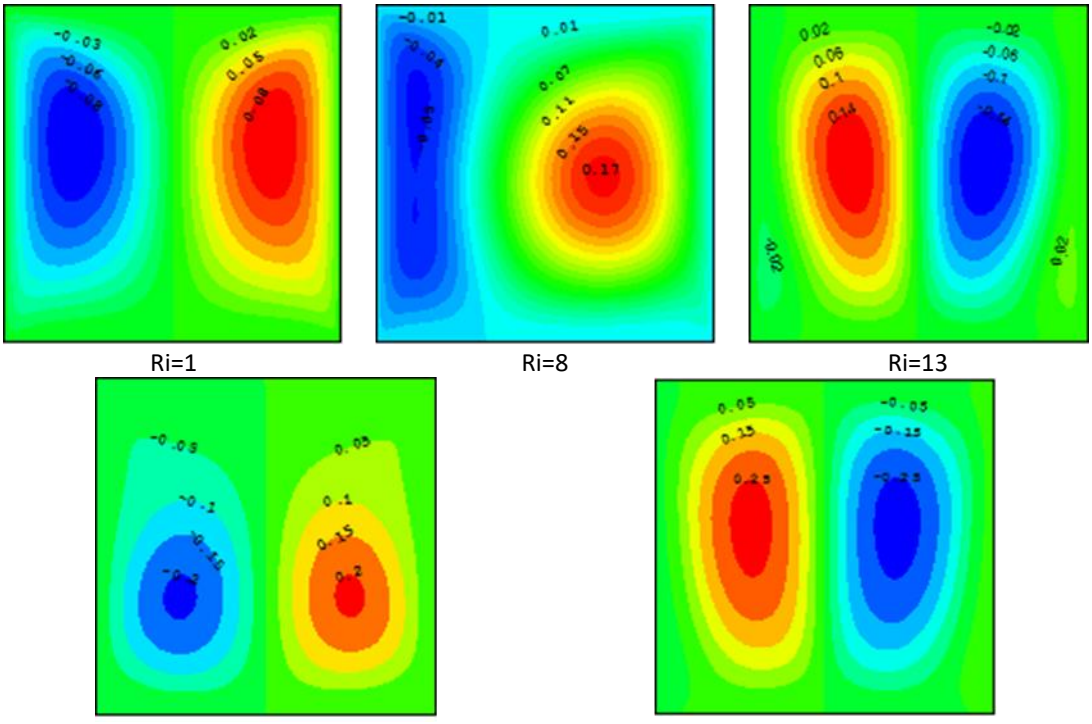

Fig. 4. Distribution of streamlines for A=1 and different values of Ri

Within the range of 4.15≤Ri≤12, increased convective activity occurs when Ri = 5, causing loss of symmetrical flow due to strengthened buoyancy forces. Although, there's typically a balance; the fluid's makeup differs, and discoveries reveal that losing cellular symmetry largely dictates heat inside the cavity.

For the Richardson numbers Ri≤4.15 (e.g., Ri=1) in Figure 6(a), the flow displays a unique structure made up of two symmetric cells. The system's symmetrical border conditions are what lead to these cells. While the left cell revolves clockwise, the right cell revolves counterclockwise. Forced convection prevails over buoyant forces in this situation, and the movement of the side walls has a big impact on the convection phenomena. It is possible to see boundary layers forming close to the moving walls. The wave shape of the isothermal lines at the cavity's center is the same. The moving side walls' shear pressures cause cooler particles to be displaced upward, resulting in this wave form.

The intensity seen in these isothermal lines is a result of this displacement. Effective heat transfer occurs in the cavity's center where buoyancy forces are modest in comparison to shearing forces. The same thing happens when the wall descends [1].

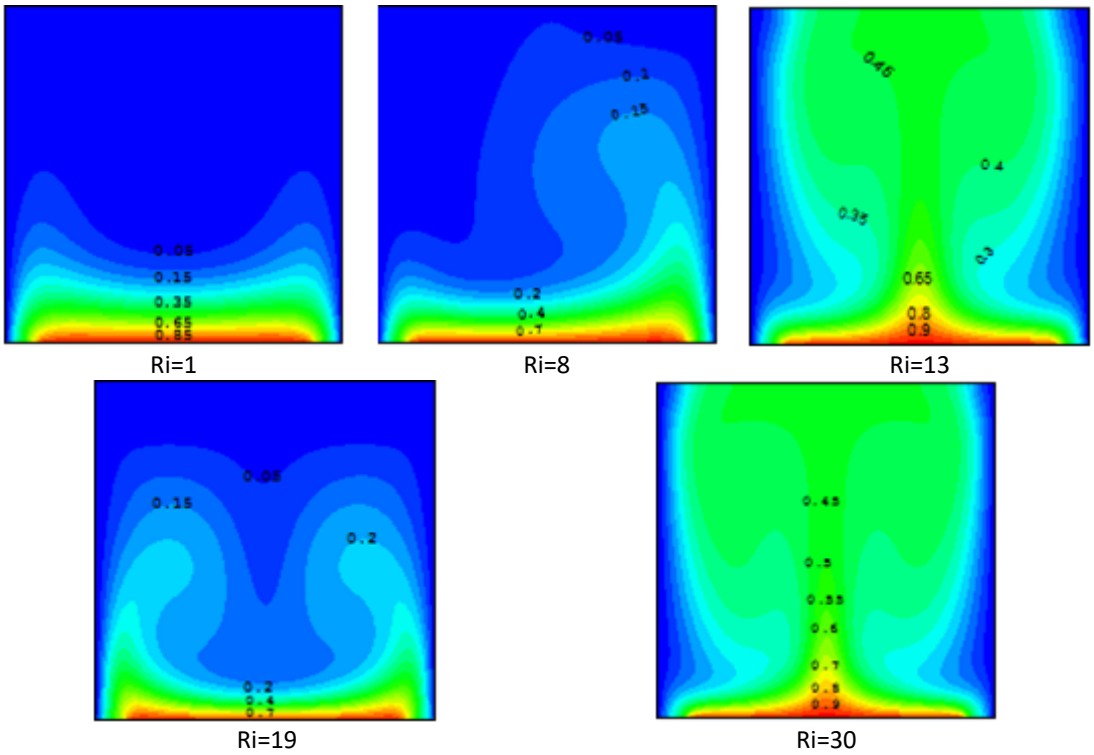

Fig. 5. Distribution of Isotherms for A=1 and different values of Ri

A second structure is where the flow enters for Richardson numbers in the range 4.15≤Ri≤12 (e.g., Ri=5). Because buoyancy forces are more powerful in this range, the convection becomes mixed and the flow loses its symmetry. Figure 6(b) shows an increase in the number of Richardson. The buoyancy and shear forces do, however, generally balance one another. The convectional heat transfer justifies the elevated temperatures within the cavity, roughly inhabiting two-thirds of the space under control of the main cell's right side with Ψmax set at 0.21, located near (X, Y) = (0.67, 0.49).

It is vital to notice that almost all of the heat recovered from the hot source in the configuration under consideration is lost via the right wall. Figure 6(a) illustrates this, showing how the usual temperature gradient at the left wall is almost zero. This suggests that there is a significant reduction in the heat transfer through the left wall.

The convection behavior becomes more logical for Richardson numbers in the range of 12≤Ri≤18 (e.g., Ri=13) for the third structure. Within this range, the flow shows a transition towards a more natural convective pattern as the Richardson number rises.

Subjected to these designated constraints (Ri = 12–18, e.g., Ri = 13), the magnitude of buoyancy forces gradually surpasses those of shear forces. Two matching sets of cells are evident in the flow's structure.

Fundamental among these cells are two complementary parts—a right cell rotating opposite the clock and an adjacent left cell rotating accordingly. It is mainly through buoyancy forces that these cells come into existence. A secondary set of cells sits adjacent to the dynamically shifting wall system. Within these cells, dense cold particles sink as buoyant warm particles climb towards the upper regions. Due to this transfer, the hotspot experiences increased temperature rise within the

chamber walls. Due to this cause, there was evidence of very hot temperatures inside the cavity (>0.35). Both sides of the building experience equal heating distribution and removal via evacuation methods, according to Figure 6(a). Characterized by a mushroom-like formation, the isothermal lines found in this building.

In the fourth structure, Richardson numbers within the range of 18≤Ri≤21 result in a dynamically active field featuring two symmetrical cells, exhibiting peak stream function value Ψ_{max}=0.21 located at X=0.75 and Y=0.35. These factors shape the thermal landscape, giving rise to two sizeable waveforms within the cavity. Conduction enhances naturally here; warmth moves from central to peripheral areas. We save cooler components near the middle section of this cavity. Finally, in the fifth structure, when Ri>21, the flow exhibits characteristics similar to the third case, with two symmetrical pairs of cells. However, these cells are more intense, as indicated by the maximum stream function value Ψ_{max}=0.27. The isothermal lines in Figure 6(a) regain the mushroom shape, but with larger dimensions. The dominant mode of convection is natural, with buoyancy forces controlling the phenomenon.

These different structures highlight the complex interplay between buoyancy and shear forces, leading to varying flow patterns and temperature distributions within the cavity.

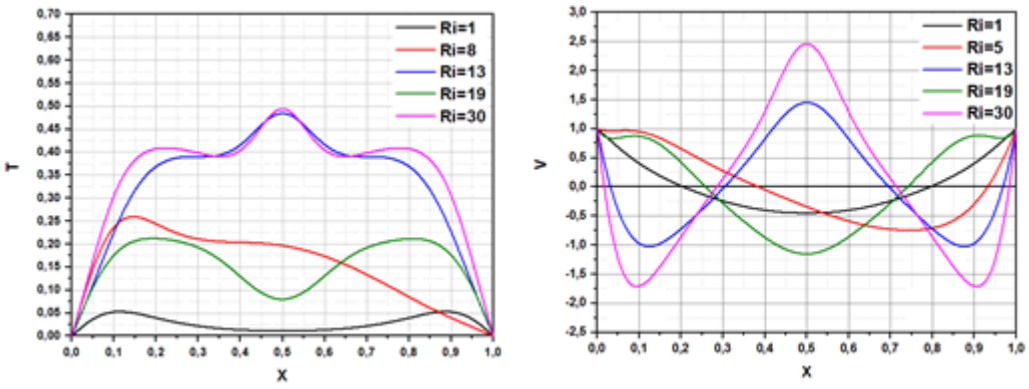

(a) (b)

Fig. 6. Variations of Temperature and V-velocity in vertical mid-plane for various values of Ri and A=1; (a) Temperature, (b) Velocity

4.2 Effect of Aspect Ratio

4.2.1 Shallow cavity

We conducted an investigation into the influence of aspect ratio in a square cavity, specifically focusing on the shallow enclosure with an aspect ratio of A=0.5. The results are presented in Figure 7 and Figure 8, which depict the streamlines and isothermal lines for various Richardson numbers, respectively. Additionally, we analyzed the variations of temperature and vertical velocity in the vertical mid-plane, as shown in Figure 9(a) and Figure 9(b).

In the shallow enclosure with A=0.5, we observed two distinct structures. The first structure occurs when the Richardson number is less than 1. In this regime, the convection is primarily driven by forced convection. The streamlines in Figure 7 reveal the presence of two symmetrical cells with a maximum stream function value Ψ_{max}=0.1. These cells, induced by shear forces, exhibit counterclockwise rotation on the right and clockwise rotation on the left. The thermal field, depicted in Figure 9(a), displays a wave-like pattern similar to the first structure observed in the square enclosure with A=1.

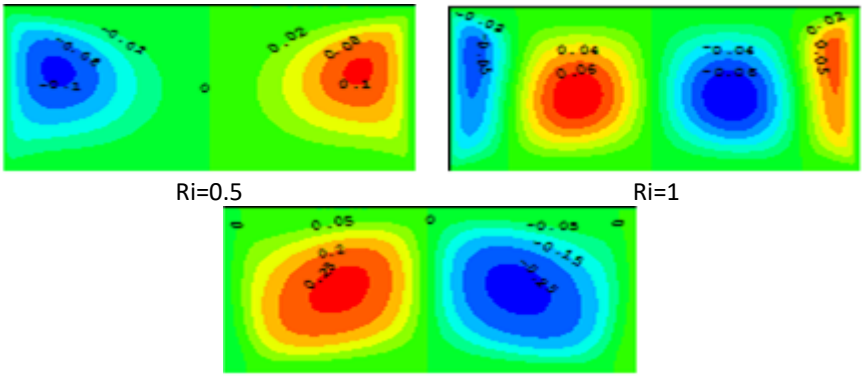

Ri=0.5 Ri=1

Ri=15

Fig. 7. Distribution of Streamlines for A=0.5 and different values of Ri

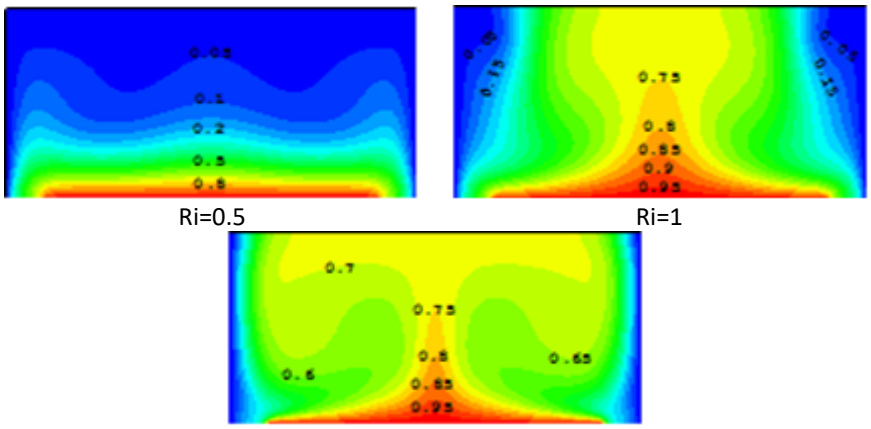

Ri=0.5 Ri=1

Ri=15

Fig. 8. Distribution of Isotherms for A=0.5 and different values of Ri

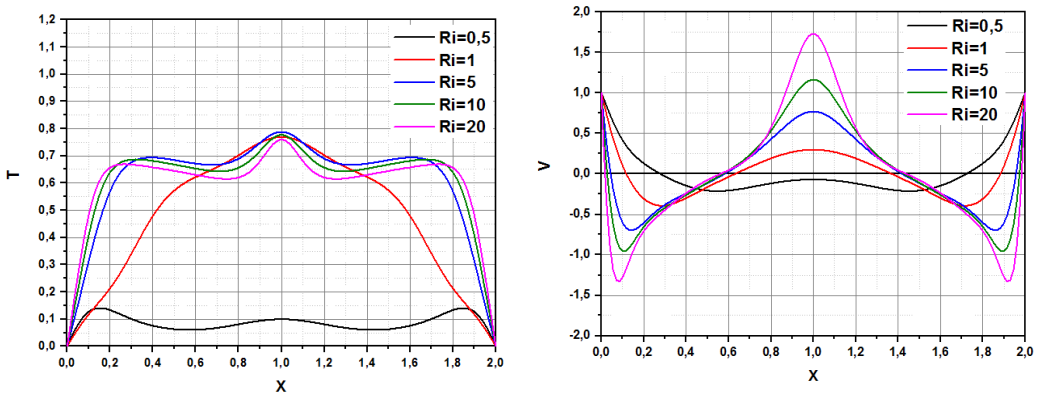

(a) (b)

Fig. 9. Variations of Temperature and V-velocity in vertical mid-plane for various values of Ri and A=0.5; (a) Temperature, (b) Velocity

In the second structure of the shallow enclosure with A=0.5, which occurs when the Richardson number is in the range of 1≤Ri≤18, the convection undergoes a transition. For example, at Ri=1, the convection becomes mixed, with the buoyancy forces balancing the shear forces within the cavity. The flow pattern is characterized by the presence of two symmetrical pairs of cells, similar to the third structure observed in the square enclosure with A=1. The maximum stream function value in these cells is Ψ_{max}=0.7. The isothermal lines in this structure exhibit a mushroom shape, and the heat transfer is evenly distributed and evacuated through both side walls. It is worth noting that as the Richardson number increases within this range (e.g., Ri=15), the convection becomes more natural

rather than mixed. In this case, the pair cells located near the walls become smaller and more intense, with a maximum stream function value of Ψ_{max}=0.27.

4.2.2 Tall cavity

In the investigation of the tall cavity with an aspect ratio of A=2, the streamlines and isothermal lines are depicted in Figure 10 and Figure 11, respectively. Additionally, Figure 12(a) and Figure 12(b) present the variations of temperature and vertical velocity in the vertical mid-plane.

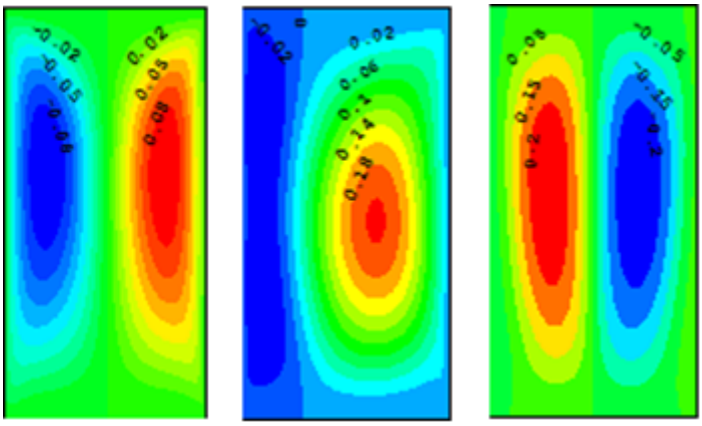

Ri=1 Ri=6 Ri=25

Fig. 10. Distribution of Streamlines for A=2 and different values of Ri

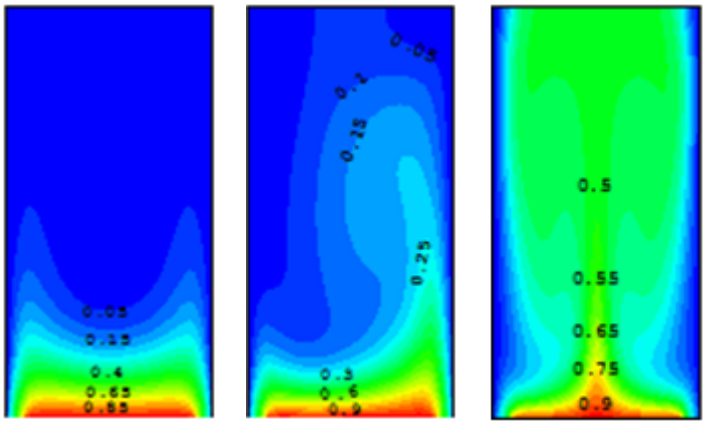

Ri=1 Ri=6 Ri=25

Fig. 11. Distribution of Isotherms for A=2 and different values of Ri

The influence of Richardson number in the tall cavity reveals three distinct flow structures. In the first structure, observed for Ri values below 4.25 (e.g., Ri=1), the flow pattern consists of two symmetrical cells. These cells are characterized by a maximum stream function value of Ψ_{max}=0.09. Consequently, the heat transfer within the cavity is considered satisfactory in this regime.

When 4.25≤Ri≤9, as in the case of the second structure of A=1 (Figure 12), the buoyancy-shear force balance has a significant impact on the flow by causing the symmetry to break down. The main cell with Ψ_{max}=0.2 (Ri=6) transported the hot particles in the right walls to the left; as Richardson increases, convection becomes more natural rather than forced and the main cell grows larger. We return to two symmetrical pairs in the third structure for Ri>9, where spontaneous convection

predominates over the central major cells produced by buoyancy forces and the small pair produced by sliding walls.

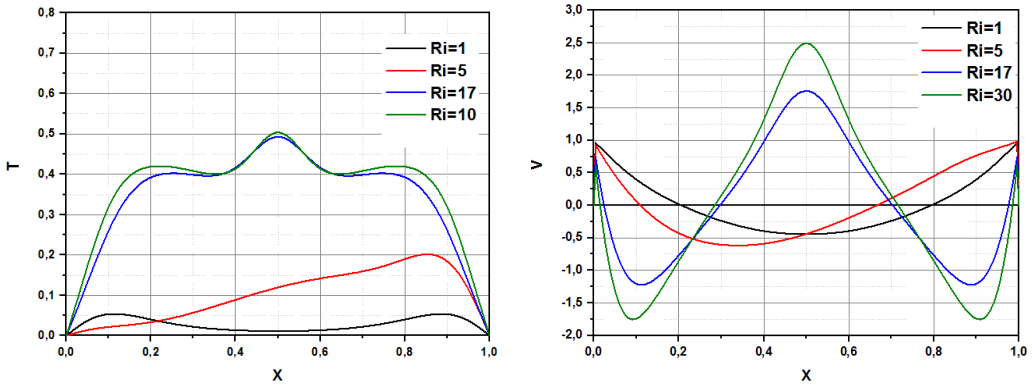

(a) (b)

Fig. 12. Variations of Temperature and V-velocity in vertical mid-plane for various values of Ri and A=2; (a) Temperature, (b) Velocity

4.3 Effect on Heat Transfer

Changes in aspect ratio, Richardson number, or ε values impact the local Nusselt number shown in Figure 13 to Figure 15, which depict a heated surface. Across diverse aspect ratios and minimal Richardson values, the profiles display symmetry. Notably, there exists an initial peak followed by descent of the Nusselt number along the surface's trajectory. Isothermal line aggregation signifies that conduction governs heat transfer (Ri = 1).

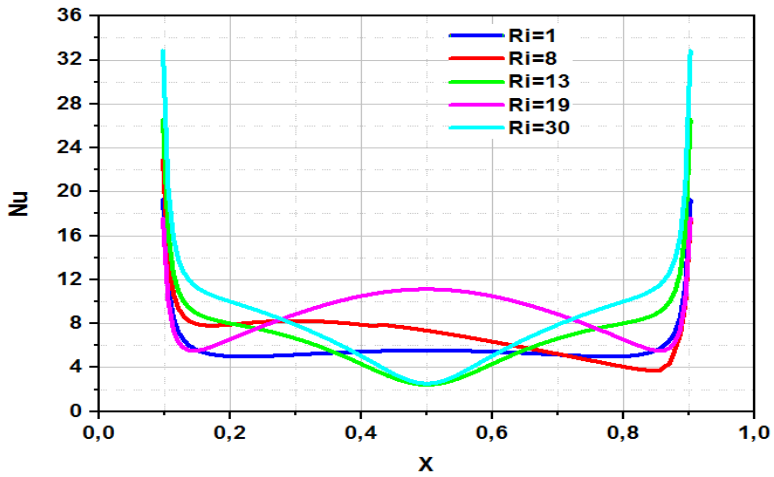

Fig. 13. Evolution of Nusselt local number for aspect ratio A=1 for various values of Ri

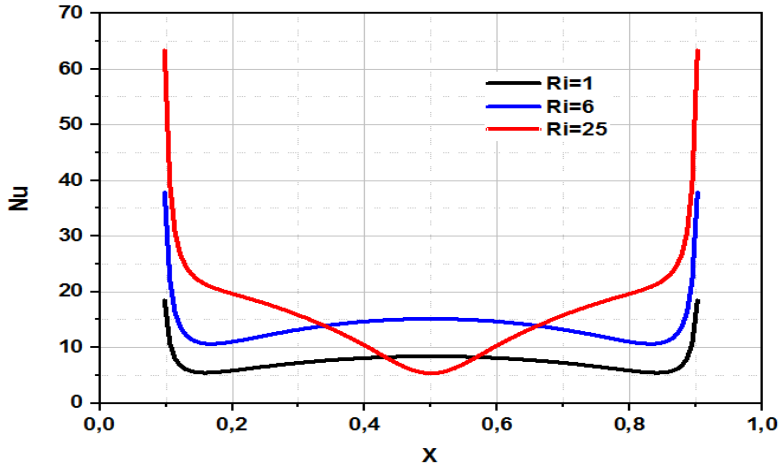

Fig. 14. Evolution of Nusselt local number for aspect ratio A=0.5 for various values of Ri

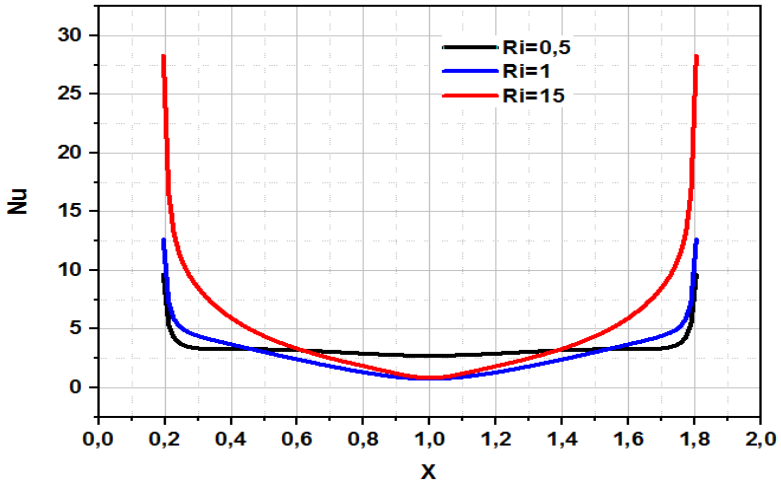

Fig. 15. Evolution of Nusselt local number for aspect ratio A=2 for various values of Ri

While symmetrical at low values, this profile manifests unique characteristics as Richardson numbers rise. Startlingly, the Nusselt number begins by being quite large along the unheated section before decreasing rapidly toward a minimum around the heated area's middle. A midway location stagnancy causes reduced convection heat transfer effectiveness.

Natural convection plays the leading role in controlling heat exchange under mixed convective conditions. Losing symmetry owing to varying dynamic fields, A=1 and A=2's curves diverge. Surface temperature increases as heat transfer intensifies to the right. By contrast, limited heat exchange takes place here; thus, there's barely any noticeable temp change nearby the left wall.

Utilizing Eq. (16) along with integral calculation via the Simpson approach grants access to the common Nusselt value. The correlation between aspect ratio adjustments and corresponding changes in average Nusselt numbers is displayed in Figure 16. Worth mentioning is how the Nusselt number signifies the proportion of convection versus conduction's heating transfer. Since the Nusselt number consistently surpasses 1, convection controls over all aspect ratios. When aspect ratio A = 1 is considered, under forced convection conditions (Ri < 4.15) heat flow sees some modest improvements.

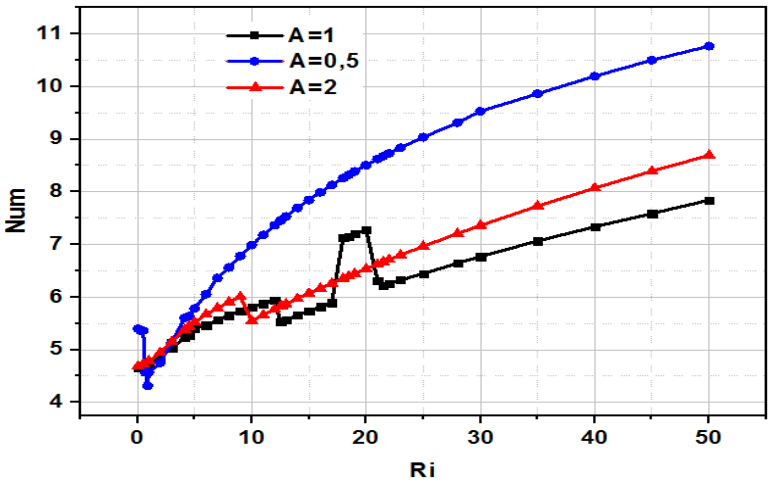

Fig. 16. Variations of average Nusselt number for various aspect ratio and Ri

As the Richardson number lies between 4.15 and 12, transition to mixed convection takes place, with subsequent increases in profile. While the Richardson number rises within the third framework, Num falls at Ri = 12. Within the scope of 12<Ri≤18, Num starts rising once more, implying a shift toward increased natural convection. A notable surge occurs in the Nusselt number across the duration of (18≤Ri≤21), climaxing in its pinnacle worth roughly 7 within the fourth frame. Once Ri reaches values beyond 18, natural convection becomes dominant, leading to subtle growth in Num. For this specific value of A (0.5), two different architectures come into view through the Nusselt number graphic display. When Ri falls below 0.7, countercurrent flow reduces heat transmission through conduction by carrying cooler elements toward the heart of the space. Contrarily, when the Richardson number surpasses 0.7 (Ri > 0.7), the convection evolves into a mixed state, leading to alterations within the flow profile and a profound rise in the Nusselt number (Num = 10.6), upon natural convection's ascendency.

In the case of a tall cavity with aspect ratio A=2, three scenarios are observed. Initially, during forced convection, the profile exhibits a slight increase. As the convection becomes mixed, the profile remains almost linear until the critical Richardson number of 9. After this point, there is a sudden decrease and subsequent increase in the profile at Ri=10, indicating a transition to natural convection. From that point onwards, the profile continues to increase, and the heat transfer is primarily controlled by natural convection.

The numerically calculated heat transfer results were correlated for mixed convection in enclosures with A=1, 2 and 0.5. Table 2 illustrate the correlated average Nusselt number as a function of the Richardson number in range of [0.05,50].

Table 2
Correlation of average Nusselt number for A=1,2,0.5 and 0.05≤Ri ≤ 50

A=0.5	0.05 ≤ Ri ≤ 0.7	0.7 < Ri ≤ 50			
Num	$4.5814\times Ri^{-0.054}$	$3.869\times Ri^{0.262}$			
A=1	0.05 ≤ Ri ≤ 4.15	4.15 < Ri ≤ 12	12 < Ri ≤ 18	18 < Ri ≤ 21	21 < Ri ≤ 50
Num	$4.625+0.073\times Ri^{1.469}$	$4.418\times Ri^{0.118}$	$3.284\times Ri^{0.206}$	$3.976\times Ri^{0.202}$	$2.686\times Ri^{0.273}$
A=2	0.05 ≤ Ri < 9	0.9 < Ri ≤ 50			
Num	$4.617+0.215\times Ri^{0.864}$	$2.805\times Ri^{0.285}$			

5. Conclusion

In the numerical simulations of mixed convection in enclosures with aspect ratios of 1, 2, and 0.5, several key findings were observed and summarized as follows

i. The Richardson number exhibited a significant influence on both the flow and heat transfer characteristics. Five different flow structures were identified within the square cavity, which presented an intriguing phenomenon for further investigation. In general, there was one structure observed during pure forced convection, two structures during mixed convection, and an additional two structures during pure natural convection. These distinct structures indicated the complex nature of the flow and heat transfer behavior.
ii. Internal cavity observations disclosed a correlation between aspect ratio and flow structure prevalence. A reduction in aspect ratio results in lower numbers of flow patterns. Contrastingly, an aspect ratio of 0.5 disclosed paired architectures, while twice that value unveiled numerous frameworks. Geometric enclosure factors influenced airflow dynamics.
iii. These findings further solidified our understanding of fluid flow dynamics thanks to the revealed connection between these two crucial factors. Increased Richardson numbers result in corresponding rises in Nusselt profiles. Decreasing the aspect ratio proved to be associated with enhanced Nusselt numbers according to the findings. Higher Richardson numbers and diminutive aspect ratios fostered improved thermal exchange inside the compartment.

Enclosure behaviors undergoing combined convection are deeply rooted in the Richardson number and dimension ratio variables analyzed in this report. Through observations of heats transfer dynamics, meaningful knowledge is gained about system optimization techniques.

References

[1] Aydin, Orhan, and Wen-Jei Yang. "Mixed convection in cavities with a locally heated lower wall and moving sidewalls." *Numerical Heat Transfer: Part A: Applications* 37, no. 7 (2000): 695-710. https://doi.org/10.1080/104077800274037
[2] Guo, Guanghong, and Muhammad A. R. Sharif. "Mixed convection in rectangular cavities at various aspect ratios with moving isothermal sidewalls and constant flux heat source on the bottom wall." *International Journal of Thermal Sciences* 43, no. 5 (2004): 465-475. https://doi.org/10.1016/j.ijthermalsci.2003.08.008
[3] Aydm, Orhan. "Aiding and opposing mechanisms of mixed convection in a shear-and buoyancy-driven cavity." *International Communications in Heat and Mass Transfer* 26, no. 7 (1999): 1019-1028. https://doi.org/10.1016/S0735-1933(99)00091-3
[4] Mohamad, A. A., and R. Viskanta. "Stability of lid-driven shallow cavity heated from below." *International Journal of Heat and Mass Transfer* 32, no. 11 (1989): 2155-2166. https://doi.org/10.1016/0017-9310(89)90122-1
[5] Oztop, Hakan F., and Ihsan Dagtekin. "Mixed convection in two-sided lid-driven differentially heated square cavity." *International Journal of Heat and Mass Transfer* 47, no. 8-9 (2004): 1761-1769. https://doi.org/10.1016/j.ijheatmasstransfer.2003.10.016
[6] Alleborn, N., H. Raszillier, and F. Durst. "Lid-driven cavity with heat and mass transport." *International Journal of Heat and Mass Transfer* 42, no. 5 (1999): 833-853. https://doi.org/10.1016/S0017-9310(98)00224-5
[7] Prasad, Ajay K., and Jeffrey R. Koseff. "Combined forced and natural convection heat transfer in a deep lid-driven cavity flow." *International Journal of Heat and Fluid Flow* 17, no. 5 (1996): 460-467. https://doi.org/10.1016/0142-727X(96)00054-9
[8] Reima, Iwatsu, Jae Min Hyun, and Kuwahara Kunio. "Convection in a differentially-heated square cavity with a torsionally-oscillating lid." *International Journal of Heat and Mass Transfer* 35, no. 5 (1992): 1069-1076. https://doi.org/10.1016/0017-9310(92)90167-Q

[9] Sharif, M. A. Rob. "Laminar mixed convection in shallow inclined driven cavities with hot moving lid on top and cooled from bottom." *Applied Thermal Engineering* 27, no. 5-6 (2007): 1036-1042. https://doi.org/10.1016/j.applthermaleng.2006.07.035

[10] Bakar, Norhaliza Abu, Rozaini Roslan, Zul Afiq Sazeli, and Nur Raidah Salim. "Mixed Convection in a Lid-Driven Cavity in the Presence of Magnetic Field with Sinusoidal Heating." *CFD Letters* 16, no. 2 (2024): 42-54. https://doi.org/10.37934/cfdl.16.2.4254

[11] Ferroudj, Nawal, Hasan Köten, and Saadoun Boudebous. "Mixed Convection Heat Transfer and Entropy Generation in a Water-filled Square Cavity Partially Heated from Below: The Effects of Richardson and Prandtl Numbers." *Journal of Applied and Computational Mechanics* 8, no. 1 (2022): 282-297.

[12] Ferroudj, Nawal, and Hasan Köten. "Numerical Simulation of Prandtl number effect on entropy generation in a square cavity." *Journal of Thermal Engineering* 7, no. 4 (2021): 1016-1029. https://doi.org/10.18186/thermal.931364

[13] Salim, Eutamene, Boudebous Saadoun, Berrahil Farid, Kholai Omar, Dahdi Bachir, and Filali Abdelkader. "Unsteady Mixed Convection in a Cubic Lid-Driven Cavity Partially Heated from the Bottom." *Journal of Advanced Research in Fluid Mechanics and Thermal Sciences* 57, no. 2 (2019): 275-287.

[14] Versteeg, Henk Kaarle. *An introduction to computational fluid dynamics the finite volume method, 2/E*. Pearson Education India, 2007.

[15] Patankar, Suhas. *Numerical heat transfer and fluid flow*. CRC Press, 2018. https://doi.org/10.1201/9781482234213

[16] Calcagni, B., F. Marsili, and M. Paroncini. "Natural convective heat transfer in square enclosures heated from below." *Applied Thermal Engineering* 25, no. 16 (2005): 2522-2531. https://doi.org/10.1016/j.applthermaleng.2004.11.032